17. Yano H, Iemura A, Haramaki M, Momosaki S, Ogasawara S, Higaki K, et al. A human combined hepatocellular and cholangiocarcinoma cell line (KMCH-2) that shows the features of hepatocellular carcinoma or cholangiocarcinoma under different growth conditions. J Hepatol 1996;24:413-422.
18. Theise ND, Yao JL, Harada K, Hytiroglou P, Portmann B, Thung SN, et al. Hepatic 'stem cell' malignancies in adults: four cases. Histopathology 2003;43:263-271.
19. Kim H, Park C, Han KH, Choi J, Kim YB, Kim JK, et al. Primary liver carcinoma of intermediate (hepatocyte-cholangiocyte) phenotype. J Hepatol 2004;40:298-304.
20. Roskams T. Anatomic pathology of hepatocellular carcinoma: impact on prognosis and response to therapy 2011. Clin Liver Dis;15: 245-259.
21. Roskams T. Liver stem cells and their implication in hepatocellular and cholangiocarcinoma. Oncogene 2006;25:3818-3822.
22. Donato R. S100: a multigenic family of calcium-modulated proteins of the EF-hand type with intracellular and extracellular functional roles. Int J Biochem Cell Biol 2001;33:637-668.
23. Hamada S, Satoh K, Hirota M, Kanno A, Ishida K, Umino J, et al. Calcium-binding protein S100P is a novel diagnostic marker of cholangiocarcinoma. Cancer Sci 2011;102:150-156.
24. Gutgemann I, Haas S, Berg JP, Zhou H, Buttner R, Fischer HP. CD56 expression aids in the differential diagnosis of cholangiocarcinomas and benign cholangiocellular lesions. Virchows Arch 2006;448:407-411.
25. Aishima S, Fujita N, Mano Y, Kubo Y, Tanaka Y, Taketomi A, et al. Different roles of S100P Overexpression in Intrahepatic Cholangiocarcinoma: Carcinogenesis of Perihilar Type and Aggressive Behavior of Peripheral Type. Am J Surg Pathol 2011;35:590-598.
26. Matsumura N, Yamamoto M, Aruga A, Takasaki K, Nakano M. Correlation between expression of MUC1 core protein and outcome after surgery in mass-forming intrahepatic cholangiocarcinoma. Cancer 2002;94:1770-1776.
27. Wang G, Platt-Higgins A, Carroll J, de Silva Rudland S, Winstanley J, Barraclough R, et al. Induction of metastasis by S100P in a rat mammary model and its association with poor survival of breast cancer patients. Cancer Res 2006;66:1199-1207.
28. van der Vegt B, de Roos MA, Peterse JL, Patriarca C, Hilkens J, de Bock GH, et al. The expression pattern of MUC1 (EMA) is related to tumour characteristics and clinical outcome of invasive ductal breast carcinoma. Histopathology 2007;51:322-335.
29. Muhlmann G, Spizzo G, Gostner J, Zitt M, Maier H, Moser P, et al. TROP2 expression as prognostic marker for gastric carcinoma. J Clin Pathol 2009;62:152-158.
30. Asayama Y, Tajima T, Okamoto D, Nishie A, Ishigami K, Ushijima Y, et al. Imaging of cholangiolocellular carcinoma of the liver. Eur J Radiol 2010;75:e120-e125.
31. Rimola J, Forner A, Reig M, Vilana R, de Lope CR, Ayuso C, et al. Cholangiocarcinoma in cirrhosis: absence of contrast washout in delayed phases by magnetic resonance imaging avoids misdiagnosis of hepatocellular carcinoma. HEPATOLOGY 2009;50:791-798.

Published OnlineFirst May 18, 2012; DOI:10.1158/1078-0432.CCR-11-2041

Cancer Therapy: Preclinical

Clinical Cancer Research

Vandetanib, an Inhibitor of VEGF Receptor-2 and EGF Receptor, Suppresses Tumor Development and Improves Prognosis of Liver Cancer in Mice

Kinya Inoue[1], Takuji Torimura[1,3], Toru Nakamura[1], Hideki Iwamoto[1], Hiroshi Masuda[1], Mitsuhiko Abe[1], Osamu Hashimoto[1], Hironori Koga[1], Takato Ueno[1], Hirohisa Yano[2], and Michio Sata[1,3]

Abstract

Purpose: VEGF, EGF, and TGF-α are expressed in hepatocellular carcinomas (HCC) and play a role in its growth. Vandetanib, a multikinase inhibitor, suppresses the phosphorylation of VEGF receptor 2 (VEGFR-2) and EGF receptor (EGFR). The aim of this study was to clarify the antitumor effect of vandetanib in mouse HCCs.

Experimental Design: We evaluated the effects of vandetanib on proliferation of human umbilical vein endothelial cells (HUVEC) and three hepatoma cell lines, as well as the phosphorylation of VEGFR-2 and EGFR in these cells. Mice were implanted with hepatoma cells subcutaneously or orthotopically in the liver and treated with 50 or 75 mg/kg vandetanib. We analyzed the effects of treatment on tumor cell proliferation and apoptosis, vessel density, phosphorylation of VEGFR-2 and EGFR, and production of VEGF, TGF-α, and EGF in tumor tissues. Adverse events on vandetanib administration were also investigated.

Results: Vandetanib suppressed phosphorylation of VEGFR-2 in HUVECs and EGFR in hepatoma cells and inhibited cell proliferation. In tumor-bearing mice, vandetanib suppressed phosphorylation of VEGFR-2 and EGFR in tumor tissues, significantly reduced tumor vessel density, enhanced tumor cell apoptosis, suppressed tumor growth, improved survival, reduced number of intrahepatic metastases, and upregulated VEGF, TGF-α, and EGF in tumor tissues. Treatment with vandetanib was not associated with serious adverse events, including alanine aminotransferase abnormality, bone marrow suppression, or body weight loss.

Conclusions: The antitumor effects of vandetanib in mice suggest that it is a potentially suitable and safe chemotherapeutic agent for HCCs. *Clin Cancer Res; 18(14); 3924–33. ©2012 AACR.*

Introduction

Hepatocellular carcinoma (HCC) is one of the most common malignant tumors in the tropics and the Far East, including Japan (1). Recently, in the SHARP trial, a phase III, randomized, placebo-controlled trial established the efficacy of sorafenib, a multikinase inhibitor, in patients with advanced HCCs (2, 3). It is known to suppress the activities of the Raf/mitogen-activated protein kinase/extracellular signal–regulated kinase (Raf/MEK/ERK) signaling pathway, tyrosine kinase VEGF receptor (VEGFR)-2, VEGFR-3, and platelet-derived growth factor receptor-β (PDGFR-β), in patients with advanced HCCs (4–6). However, the benefits of sorafenib are limited to prolongation of survival for only 3 months. Thus, other molecular target agents are required for the treatment of advanced HCCs.

Tumor growth and formation of metastases are dependent on the existence of adequate blood supply (7, 8).

In HCCs, the tumor tissue is supplied by blood from new arteries and the development of rich vasculature occurs in parallel with tumor development (9). VEGF plays a critical role in the process of angiogenesis (10, 11). VEGF is produced by hepatoma cells, hepatic stellate cells, and endothelial cells, and its expression level correlates with tumor growth (12). Hepatoma cells also produce EGF and TGF-α and express EGF receptor (EGFR; ref. 13). Increasing evidence has highlighted the importance of EGFR and its ligands EGF and TGF-α in hepatocarcinogenesis (14, 15).

Vandetanib (Zactima; ZD6474) is an orally bioavailable, small-molecule VEGFR-tyrosine kinase inhibitor with additional activity against EGFR-tyrosine kinase and RET receptor tyrosine kinase (16). Therefore, vandetanib, in addition to inhibiting endothelial cell proliferation through the

Authors' Affiliations: [1]Division of Gastroenterology, Department of Medicine, [2]Department of Pathology, Kurume University School of Medicine, and [3]Liver Cancer Division, Research Center for Innovative Cancer Therapy, Kurume University, Fukuoka, Japan

Note: Supplementary data for this article are available at Clinical Cancer Research Online (http://clincancerres.aacrjournals.org/).

Corresponding Author: Takuji Torimura, Liver Cancer Division, Research Center for Innovative Cancer Therapy, Kurume University, 67 Asahi-machi, Kurume City, Fukuoka 830-0011, Japan. Phone: 81-942-317746; Fax: 81-942-317747l; E-mail: tori@med.kurume-u.ac.jp

doi: 10.1158/1078-0432.CCR-11-2041

Published OnlineFirst May 18, 2012; DOI:10.1158/1078-0432.CCR-11-2041

Translational Relevance

VEGF plays the significant role of vascular development in hepatocellular carcinomas (HCC). Recently, several clinical trials of molecular-targeted agents for advanced HCCs have been investigated. On the basis of their results, it has been proved that antiangiogenic agents such as sorafenib are effective for advanced HCCs. However, their efficacies are not fully satisfied yet. EGF receptor signaling is upregulated in HCCs. Vandetanib, a multi-tyrosine kinase inhibitor, is known to suppress the phosphorylation of EGF receptor and VEGF receptor-2 (VEGFR-2). Here, we show for the first time that vandetanib suppressed tumor growth, intrahepatic metastasis and prolonged the survival of mouse HCC model and that these effects are mainly mediated by inhibition of vascular formation. In addition, vandetanib was effective for enlarged mouse HCC model. These preclinical results suggest that vandetanib could be potentially useful for patients with advanced HCCs.

blockade of VEGF-induced signaling, can suppress tumor cell growth more directly through the blockade of EGFR autocrine signaling (17).

The present study was designed to assess the antitumor effects and adverse effects of vandetanib in mouse HCC models.

Materials and Methods

Reagents, cells, and animals

We used 3 hepatoma cell lines, HAK1-B, HuH-7, and KYN-2. Human umbilical vein endothelial cells (HUVEC) and HuH-7 were obtained from CAMBREX Bio Science Walkersville Inc. KYN-2 (18) and HAK1-B (19) were obtained from the Department of Pathology of our university. Male 5-week-old nude mice (BALB/c *nu/nu*; Kyudo KK.) and mice with severe-combined immunodeficiency (SCID; CB-7/1cr, Kyudo KK.) were acclimatized and placed in separate cages. All animals received humane care according to the guideline of the NIH for the Policy on Humane Care and Use of Laboratory Animals. The experimental protocol was approved by the Laboratory Animal Care and Use Committee of Kurume University (Fukuoka, Japan).

In vitro inhibition of cell proliferation by vandetanib

Approximately 1,000 HUVECs in 200 μL of endothelial cell growth medium-2 (EGM-2) medium (EGM-2 Bullet Kit; Clonetics) supplemented with 5% FBS were added to each well of 96-well plastic dishes and incubated at 37°C for 24 hours. The medium was replaced with 200 μL of EBM-2 with 5% FBS containing various concentrations of vandetanib (0, 0.01, 0.05, 0.1, 0.5, 1.0, 10.0 μmol/L). After incubation for 30 minutes, VEGF (3 ng/mL) was added. In another experiment, approximately 1,000 hepatoma cells in 200 μL of Dulbecco's Modified Eagle's Medium (DMEM; Gibco Invitrogen Cell Culture) supplemented with 10% FBS were added to each well of 96-well plastic dishes and incubated at 37°C for 24 hours. The medium was replaced with 200 μL of medium containing various concentrations of vandetanib (0, 0.05, 0.1, 0.5, 1.0, 5.0, 10.0 μmol/L). After incubation for 72 hours, cell proliferation was measured by a tetrazolium-based assay (Cell Count Reagent SF; Nacalai Tesque Inc.). Then, we conducted cell-cycle analysis of 3 hepatoma cell lines by flow cytometry. After incubation for 72 hours with vandetanib (0, 10 μmol/L), the floating and attached cells were harvested and washed with PBS. The DNA content was assessed by staining ethanol-fixed cells with propidium iodide and monitoring by FACSCalibur (Becton Dickinson). The percentage of cells in the sub-G_0/G_1 population was determined using CellQuest software (BD).

Western blotting

HUVECs were cultured in serum-free and VEGF-free medium, and hepatoma cells were cultured in serum-free medium for 12 hours. HUVECs were treated with various concentrations of vandetanib (0, 1.0, 5.0, 10.0 μmol/L) for 60 minutes and then incubated with VEGF (0, 50 ng/mL) for 5 minutes. Hepatoma cells were treated with vandetanib (0, 1.0, 5.0, 10.0 μmol/L) for 60 minutes and then incubated with EGF (0, 100 ng/mL) for 5 minutes. Total cell protein (50 μg) and tissue lysates were run on 10% SDS-PAGE and transferred to polyvinylidene difluoride membranes. The membranes were incubated overnight at 4°C with rabbit anti-phosphorylated VEGFR-2 antibody (Ty1175; Cell Signaling Technology Inc.), rabbit anti-VEGFR-2 antibody (Calbiochem-Novabiochem Corporation), rabbit anti-phosphorylated EGFR (Ty1173; Cell Signaling Technology Inc.), rabbit anti-EGFR (Cell Signaling Technology), rabbit anti-VEGF antibody (Abcam Japan), rat anti-EGF antibody (Monosan), rabbit anti-TGF-α antibody (Abcam Japan), and mouse anti-actin antibody (Sigma-Aldrich, Inc.). Each antibody was diluted 500-fold. After incubation with secondary donkey anti-rabbit horseradish peroxidase (HRP)-conjugated IgG (dilution, 1:10,000 dilution; GE Healthcare Bio-Sciences GK), anti-rat HRP-conjugated mouse IgM (dilution, 1:2,000; Zymed Laboratories), or donkey anti-mouse HRP-conjugated IgG (dilution, 1:5,000; GE Healthcare Bio-Sciences GK) for 1 hour, immunoreactive bands were stained by an enhanced chemiluminescence Western blot analysis system (Amersham Pharmacia Biotech).

Protocols of tumor growth studies of subcutaneous tumor models

Tumor cells (5×10^6) were injected subcutaneously into the dorsal side in nude mice. The tumor-bearing mice were randomly divided into PBS-treated group ($n = 6$) and vandetanib-treated groups ($n = 6$). Treatment was initiated when the average size of the tumor reached 50 to 100 mm^3; the tumor-bearing mice were orally administered PBS or vandetanib (50 or 75 mg/kg) every day. To evaluate the

Published OnlineFirst May 18, 2012; DOI:10.1158/1078-0432.CCR-11-2041

antitumor effect of vandetanib in mice bearing large tumors of HuH-7 (>500 mm^3), the mice received PBS ($n = 6$) or vandetanib (75 mg/kg; $n = 6$). Two dimensions of the tumor were measured by calipers every 3 days, and the tumor volume was calculated by the equation: length × $width^2 \times 0.52$.

Protocols of growth, survival, and intrahepatic metastases studies of liver tumor models

For tumor growth studies, nude mice were injected with KYN-2 into the liver. The mice were randomly divided into PBS-treated group ($n = 6$) and vandetanib-treated groups (50 mg/kg, $n = 6$; 75 mg/kg, $n = 6$). After 7 days, the mice were treated orally with vandetanib every day for 3 weeks. They were subsequently sacrificed at day 28, and tumor volume was evaluated.

For survival studies, KYN-2 cells were implanted into another group of 12 nude mice, which were then randomly divided into PBS-treated group ($n = 6$) and vandetanib-treated group (75 mg/kg; $n = 6$). Mice were sacrificed according to the clinical signs of weakness, anorexia, or more than 20% weight loss.

To evaluate intrahepatic metastasis, 2×10^6 KYN-2 cells were implanted into the liver of SCID mice. The mice were then randomly divided into PBS-treated group ($n = 6$) and vandetanib-treated group (75 mg/kg; $n = 6$). Administration of vandetanib for 3 weeks was followed by counting the number of intrahepatic nodules.

Assessment of vascular density, proliferation activity, and apoptotic index in tumor tissues of liver tumor model

The sections of liver tumor tissues were incubated with rabbit anti-mouse CD31 antibody (dilution, 1:100; Abcam Japan) and rabbit anti-PCNA antibody (dilution, 1:100; Santa Cruz Biotechnology, Inc.) at 4°C overnight. Then, the sections were incubated with fluorescein isothiocyanate (FITC)-conjugated (dilution, 1:100) or EnVision+System-HRP-labeled polymer anti-rabbit (Dako Japan). The sections were also examined for apoptosis of tumor cells by terminal deoxynucleotidyl transferase–mediated dUTP nick end labeling (TUNEL) staining with In Situ Apoptosis detection kit (Oncor). The numbers of CD31-positive blood vessels in tumor tissues were counted in 50 blindly selected random fields (z-series, ×63 oil magnification). Proliferating cell nuclear antigen (PCNA)- and TUNEL-positive cells among 1,000 hepatoma cells were counted in 28 blindly selected random fields.

Measurement of serum levels of α-fetoprotein, vandetanib, alanine aminotransferase, bone marrow functions, and body weight

Serum α-fetoprotein (AFP) levels were measured at the time of sacrifice in tumor-bearing mice. Serum levels of vandetanib were measured by high-performance liquid chromatography (HPLC) at the time of sacrifice. We also determined leukocyte and platelet counts, hemoglobin (Hb) levels, and serum alanine aminotransferase (ALT) levels. Body weight was evaluated at the start of treatment and at sacrifice.

Statistical analysis

All data were expressed as mean ± SD. Differences between groups were examined for statistical significance using the Mann–Whitney *U* test, the Kruskal–Wallis rank test, and the log-rank test. A *P* value less than 0.05 denoted the presence of a statistically significant difference.

Results

Vandetanib inhibits endothelial cell and hepatoma cell proliferation

Vandetanib suppressed cell proliferation of HUVECs (IC_{50} = 7.1 μmol/L) from 0.01 μmol/L of vandetanib in a dose-dependent manner (Fig. 1A). It also suppressed cell proliferation of the human hepatoma cell line (HAK1-B; IC_{50} = 10.0 μmol/L) in a dose-dependent manner from 0.05 μmol/L of vandetanib (Supplementary Fig. S1A). Vandetanib also suppressed the proliferation of KYN-2 cells (IC_{50} = 8.1 μmol/L) and HuH-7 cells (IC_{50} = 9.4 μmol/L) from 5 to 10 μmol/L of vandetanib (Supplementary Fig. S1B and S1C). The rates of apoptosis of vandetanib-treated hepatoma cells (HAK1-B, 74.3%; KYN-2, 41.8%; HuH-7, 62.5%) were higher than those of nontreated hepatoma cells (HAK1-B, 20.4%; KYN-2, 10.7%; HuH-7, 31.3%; Fig. 1B).

Vandetanib inhibits phosphorylation of VEGFR-2 and EGFR

Vandetanib (at both 5 and 10 μmol/L) significantly inhibited VEGFR-2 phosphorylation in HUVECs (Fig. 1C). Although vandetanib (at 1–10 μmol/L) suppressed EGFR phosphorylation in the 3 hepatoma cell lines (Fig. 1D; Supplementary Fig. S2A and S2B), it did not affect the expression of total VEGFR-2 and EGFR in the same cells.

Vandetanib inhibits tumor growth of hepatoma cells in subcutaneous tumor model

In the HuH-7 xenograft model, the tumor volumes at baseline of the PBS group and 50 and 75 mg/kg vandetanib groups were 63.5 ± 11.9, 70.3 ± 16.2, and 72.3 ± 11.6 mm^3, respectively. After 3 weeks of treatment, the respective tumor volumes were 4,704.7 ± 2,205.4, 773.4 ± 458.5, and 279.4 ± 91.9 mm^3, respectively (Fig. 2A). In another experiment, treatment commenced when tumor volume was more than 500 mm^3. Before treatment, the tumor volumes were 570.0 ± 95.6 mm^3 and 614.5 ± 169.2 mm^3 in the PBS and 75 mg/kg vandetanib groups, respectively. After 15 days of treatment, the respective tumor volumes were 2,491.1 ± 1,451.9 and 572.2 ± 441.5 mm^3 (Fig. 2B).

In the HAK1-B xenograft model, the tumor volumes before treatment of the PBS and 50 mg/kg vandetanib groups were 68.8 ± 12.2 and 75.6 ± 15.4 mm^3, respectively.

Published OnlineFirst May 18, 2012; DOI:10.1158/1078-0432.CCR-11-2041

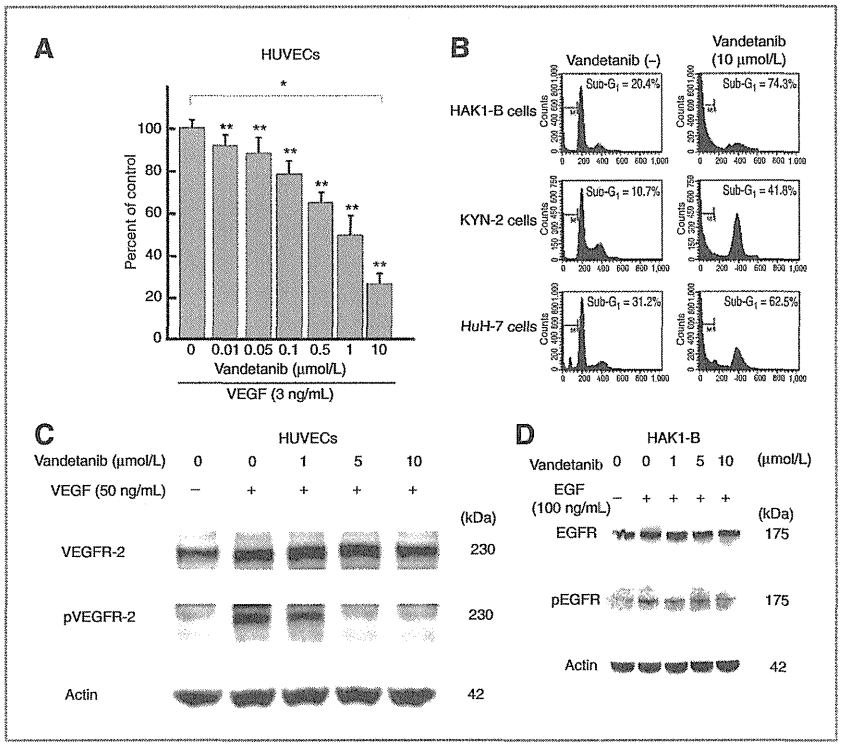

Figure 1. Inhibitory effects of vandetanib on cell proliferation, and phosphorylation of VEGFR-2 and EGFR. A, HUVECs were cultured with a medium containing vandetanib, FBS, and VEGF. Seventy-two hours later, cell proliferation was evaluated by the tetrazolium-based assay. B, hepatoma cells were cultured with a medium containing vandetanib (0, 10 μmol/L) and FBS. Seventy-two hours after incubation, ethanol-fixed floating and attached cells were stained with propidium iodide. Cell apoptosis and cell cycle were determined by flow cytometry. C, HUVECs were cultured in the medium containing vandetanib and VEGF. D, HAK1-B hepatoma cells were cultured in a medium containing vandetanib and EGF. Data are mean ± SD. *, $P < 0.05$, compared with the control by Kruskal–Wallis test; **, $P < 0.05$, compared with the control by Mann–Whitney *U* test. pEGFR, phosphorylated EGFR; pVEGFR-2, phosphorylated VEGFR-2.

After 3 weeks, the respective tumor volumes were 461.4 ± 134.9 and 169.8 ± 37.8 mm^3 (Fig. 2C). In the KYN-2 xenograft model, the tumor volumes before treatment of the PBS and 50 mg/kg vandetanib groups were 56.7 ± 12.0 and 62.6 ± 13.3 mm^3, respectively, which increased at 3 weeks after the treatment to 10,092.9 ± 7,795.3 and 1,434.4 ± 903.1 mm^3, respectively (Fig. 2D).

Vandetanib inhibits tumor growth and phosphorylation of VEGFR-2 and EGFR

In mice implanted with KYN-2 cells, tumor volume showed a significant inverse relationship with the dose of administered vandetanib (PBS group, 2,137.4 ± 873.3 mm^3; 50 mg/kg vandetanib group, 928.9 ± 515.5 mm^3; 75 mg/kg vandetanib group, 295.5 ± 427.6 mm^3; Fig. 3A; Supplementary Fig. S3A). Serum AFP levels were 50,567 ± 11,300 and 16,540 ± 14,297 ng/mL in the PBS and 75 mg/kg vandetanib groups, respectively (Supplementary Fig. S3B). In tumor-bearing mice treated with vandetanib, tumor tissues showed significant suppression of VEGFR-2 and EGFR phosphorylation (Fig. 3B and C). The production levels of VEGF, TGF-α, and EGF were significantly upregulated in the 50 and 75 mg/kg vandetanib-treated groups compared with the PBS-treated group (Fig. 3D).

Vandetanib prolongs survival of tumor-bearing mice

The survival time ranged from 55 to 75 days (mean, 66.4 ± 8.6 days) in mice bearing tumors of KYN-2 treated with 75 mg/kg vandetanib. This was significantly longer than that of PBS-treated mice (range, 28–62 days; mean, 40.5 ± 11.7 days; Fig. 4A). However, all tumor-bearing mice ultimately died of tumor growth.

Vandetanib inhibits intrahepatic tumor metastasis

In the PBS group, the number of tumor nodules in livers implanted with KYN-2 cells ranged from 4 to 16 (mean, 7.7 ± 4.5). Treatment with 75 mg/kg vandetanib significantly reduced the number of tumor nodules (range, 3–4; mean, 3.2 ± 0.4; Fig. 4B).

Serum vandetanib levels and inhibition of tumor vascularization

Serum vandetanib levels in mice treated with 50 and 75 mg/kg ranged from 2.5 to 14.1 μmol/L (mean, 7.3 ± 4.6)

Published OnlineFirst May 18, 2012; DOI:10.1158/1078-0432.CCR-11-2041

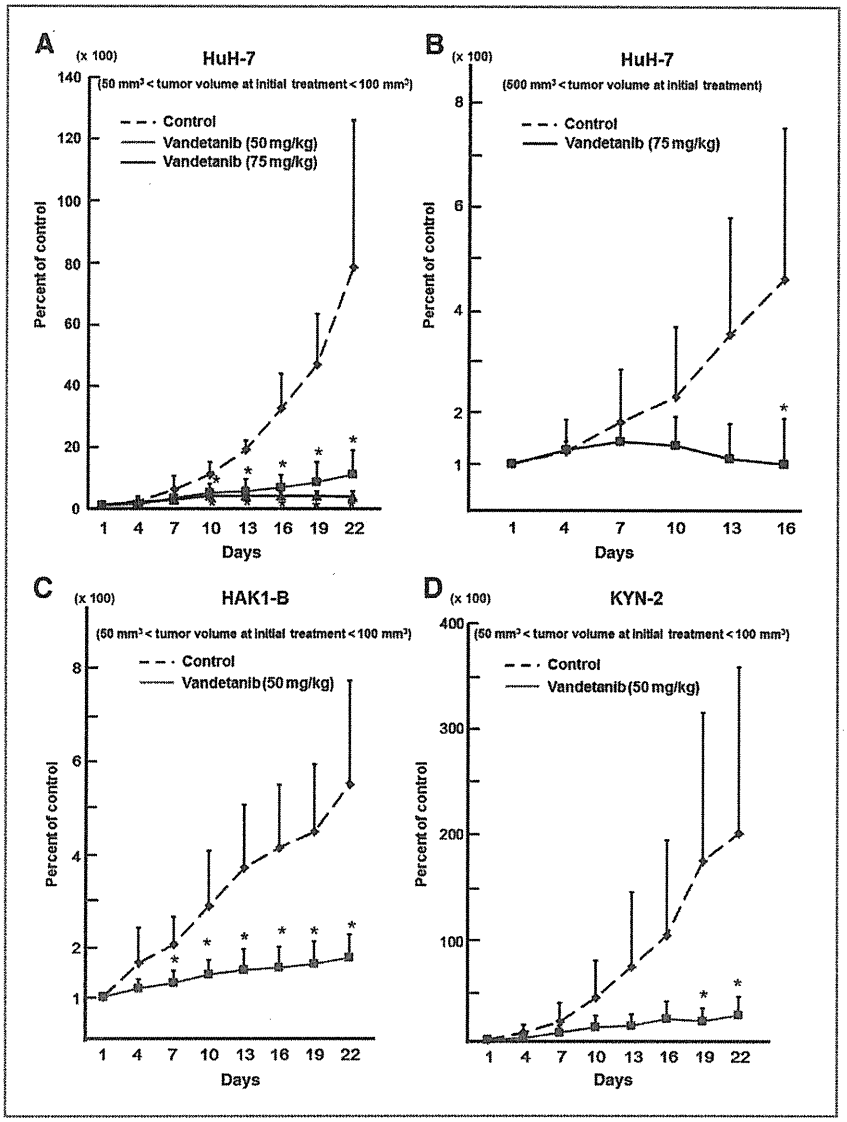

Figure 2. Serial changes in tumor growth induced by treatment with vandetanib in mice carrying subcutaneously implanted human hepatoma cell tumors. Mean ± SD tumor volume is expressed as percentage of the control ($n = 6$ per group). A, HuH-7 cells: treatment commenced when tumor volume was 50 to 100 mm^3. *, $P < 0.05$, compared with PBS-treated mice by Mann–Whitney U test. B, HuH-7: treatment commenced when tumor volume was more than 500 mm^3 to evaluate antitumor effect of vandetanib on enlarge tumors. *, $P < 0.05$, compared with PBS-treated mice by Mann–Whitney U test. (C) HAK1-B and (D) KYN-2: treatment commenced when tumor was 50 to 100 mm^3. *, $P < 0.05$, compared with PBS-treated mice by Mann–Whitney U test.

and 3.8 to 12.7 μmol/L (mean, 8.5 ± 3.0) at the time of sacrifice, respectively. The mean number of vessels in tumor tissues of the PBS, 50 and 75 mg/kg vandetanib groups were 15.6 ± 7.4 per high-power field (HPF), 9.3 ± 2.9 per HPF, and 6.0 ± 2.4 per HPF, respectively. Vandetanib suppressed vascular development in a dose-dependent manner (Fig. 5A and B). The vascular density in these tumors correlated with tumor volume (data not shown).

Effects of vandetanib on cell proliferation and apoptosis in tumor tissues

Vandetanib had not effect on cell proliferation of hepatoma cells (data not shown), but it increased the apoptotic index in tumor tissues from 1.2% ± 0.7% in the PBS to 2.5% ± 0.7% and 3.1% ± 0.9% in the 50 and 75 mg/kg treatment groups, respectively. The effect of vandetanib on apoptosis was dose-dependent.

Effects of vandetanib on serum ALT, body weight, and bone marrow function

There was no significant difference in body weight between the start and end of treatment in the PBS group, 50, and 75 mg/kg vandetanib groups. There were also no significant differences in body weight of the 3 groups at the start of treatment and at sacrifice (Fig. 6A). There were also no significant differences of serum ALT levels, leukocyte count, platelet count, and Hb levels among the 3 groups at sacrifice (Fig. 6B and C).

Published OnlineFirst May 18, 2012; DOI:10.1158/1078-0432.CCR-11-2041

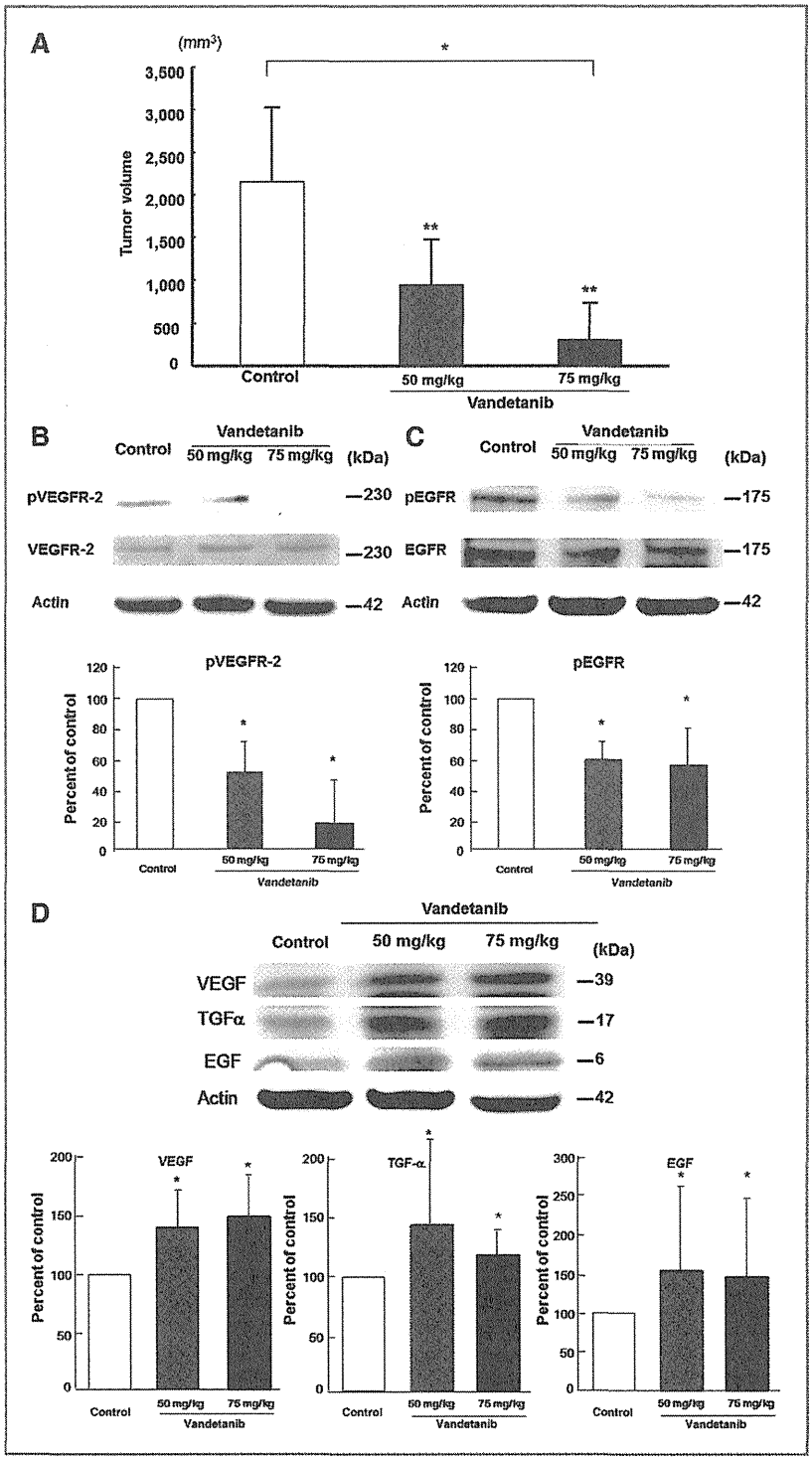

Figure 3. Vandetanib inhibits tumor growth in the liver in nude mice. A, comparison of tumor volume. Tumor volumes are expressed as mean ± SD ($n = 6$ per group). *, $P < 0.05$, by Kruskal-Wallis test; **, $P < 0.05$, by Mann–Whitney U test compared with PBS-treated mice. B, expression of pVEGFR-2 and VEGFR-2. C, Expression of pEGFR and EGFR. D, expression of VEGF, TGF-α, and EGF. Tissue lysate protein (50 μg) was run on 10% SDS-PAGE. pEGFR, phosphorylated EGFR; pVEGFR-2; phosphorylated VEGFR-2.

Published OnlineFirst May 18, 2012; DOI:10.1158/1078-0432.CCR-11-2041

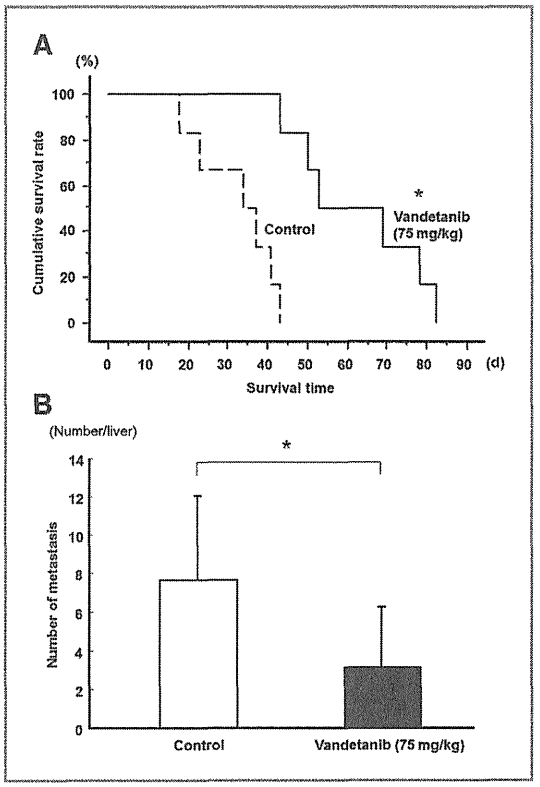

Figure 4. Beneficial effects of vandetanib on the survival time and the intrahepatic metastasis in mice implanted with KYN-2 cells. A, Kaplan–Meier estimates of survival in mice treated with vandetanib (75 mg/kg) compared with those treated with PBS. The survival time was counted from the day of tumor cell transplantation. *, $P < 0.05$, compared with PBS-treated mice by log-rank test. B, numbers of tumor nodules in the liver were counted after 28 days of KYN-2 cells implantation and expressed as mean ± SD ($n = 6$ per group). *, $P < 0.05$, compared with PBS-treated mice by Mann–Whitney U test.

Discussion

In general, signal transduction through VEGFR-2 participates in endothelial cell proliferation much more than VEGFR-1 (20). Gule and colleagues (16) reported that the antitumor effects of vandetanib were mediated through inhibition of VEGF signaling and antiangiogenesis rather than through direct antiproliferative effects on tumor cells. In our *in vivo* study, vandetanib dose dependently suppressed the phosphorylation of VEGFR-2 and microvascular development. Furthermore, vandetanib also induced apoptosis of hepatoma cells *in vivo*, although it did not suppress the proliferation of hepatoma cells. O'Reilly and colleagues (21) reported that antiangiogenic therapy upregulated the apoptotic index of tumor cells but did not reduce the proliferation of tumor cells. The above results suggest that vandetanib mainly suppresses tumor growth through its tumor antiangiogenic effect by inhibition of VEGF signaling rather than suppressing the proliferation of tumor cells. In our study, however, vandetanib at relatively high concentrations suppressed cell proliferation and increased apoptosis of hepatoma cells *in vitro*. In addition to EGF, fibroblast growth factor (FGF), and PDGF also participate in hepatoma cell proliferation (22, 23). At relatively high concentrations, vandetanib inhibits FGFR and PDGFR kinases (24). Because serum vandetanib levels were relatively high, high rate of apoptosis *in vivo* might be induced through inhibition of EGF and PDGF signaling, as well as FGF signaling. Thus, the inhibition of these signaling pathways seems important for the effects of vandetanib in the mouse HCC model, in addition to the inhibition of VEGF signaling.

In the orthotopic liver tumor xenograft model, which mirrors the clinical course of hepatoma more accurately than the subcutaneous xenograft model, serum vandetanib levels in 50- and 75 mg/kg–treated mice were not significantly different. However, tumor volume was significantly suppressed in a dose-dependent manner. In addition, vandetanib prolonged the survival time of tumor-bearing mice. It also suppressed the growth of larger HuH-7 xenografts. These findings suggest that vandetanib is potentially useful for patients with advanced HCCs. However, our study did

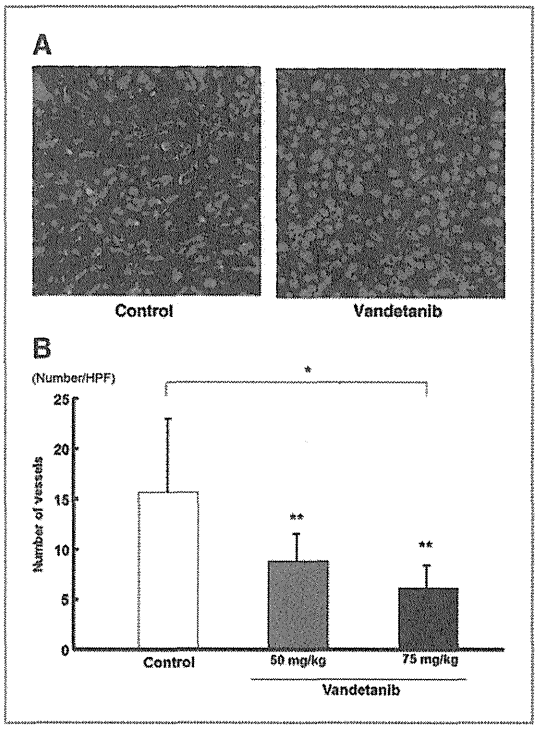

Figure 5. Effect of vandetanib on tumor vascularization. A, immunohistochemical analysis showed fewer CD31-positive vessels in tumor tissues of mice treated with vandetanib compared with the PBS-treated mice. B, the density of CD31-positive vessels in a tumor field is represented as mean ± SD (50 fields of 18 sections from each of 6 tumors). *, $P < 0.05$, compared with PBS-treated group by Kruskal–Wallis test; **, $P < 0.05$, compared with PBS-treated group by Mann–Whitney U test.

Published OnlineFirst May 18, 2012; DOI:10.1158/1078-0432.CCR-11-2041

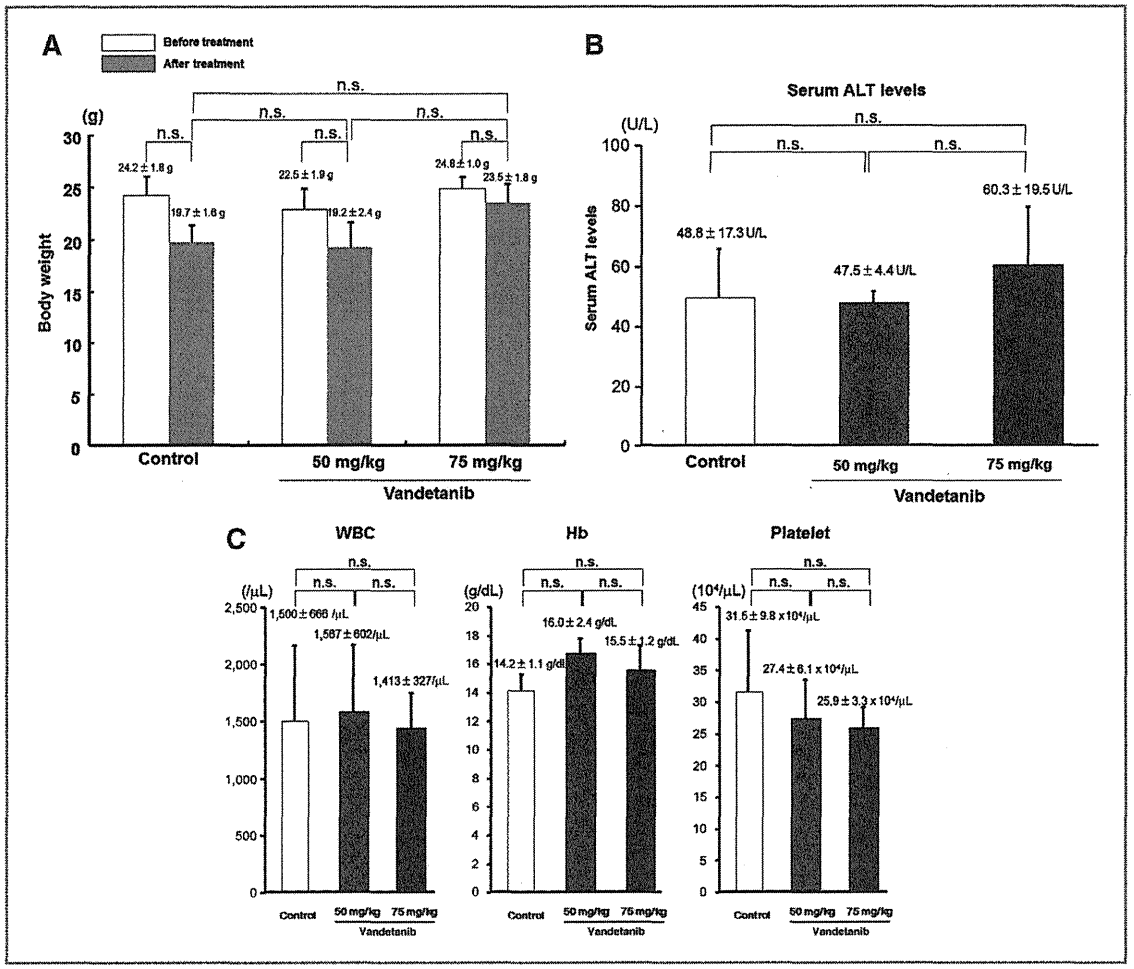

Figure 6. Effects of vandetanib on body weight, serum ALT levels, and bone marrow function in tumor-bearing mice. A, body weight of tumor-bearing mice in the PBS- and vandetanib-treated groups (50 and 75 mg/kg) at the start of treatment and at sacrifice. There was no significant difference in body weight between start of treatment and at sacrifice in each group. B, serum ALT levels in mice treated with PBS and vandetanib (50 and 75 mg/kg). C, leukocyte count, Hb level, and platelet count in PBS- and vandetanib-treated mice (50 and 75 mg/kg). Vandetanib did not result in any significant change in all 4 parameters. n.s., not significant; WBC, white blood cells.

not provide answers to why the antitumor effect of 75 mg/kg vandetanib was superior to that of 50 mg/kg even though the serum levels were not significantly different. Further studies of pharmacodynamics of vandetanib are needed.

Our results also showed that vandetanib significantly suppressed intrahepatic metastasis of KYN-2 cells. In their *in vitro* study, Giannelli and colleagues (25) reported that vandetanib blocked the proliferation, adhesion, migration, and invasion of hepatoma cells via inhibition of the EGFR pathway. Several studies have investigated tumor cell proliferation and metastasis (16, 25, 26), as well as the correlation between angiogenesis and tumor metastasis (27). What are the mechanisms of vandetanib-induced suppression of intrahepatic macrometastasis? While no direct mechanism was identified, our study showed 3 possible mechanisms. First, vandetanib suppresses tumor cell migration from the primary tumor by inhibiting primary tumor growth and expansion. Second, vandetanib inhibits the EGFR pathway and thus suppresses the adhesion, migration, and invasion of hepatoma cells (28), which are critical steps in the metastatic process. Third, vandetanib inhibits metastatic tumor enlargement ensuring inactivity of micrometastases (29).

Vandetanib administration did not reduce body weight, increase ALT, induce bone marrow suppression, or cause other serious adverse events. Recent clinical studies on the use of vandetanib in patients with lung cancer, the most common adverse events that resulted in discontinuation of vandetanib were diarrhea, rashes, and QTc prolongation (30). In the present study, we did not experience severe

Published OnlineFirst May 18, 2012; DOI:10.1158/1078-0432.CCR-11-2041

diarrhea and skin rash in tumor-bearing nude mice. These differences could represent differences in species.

Several types of molecular-targeted agents are currently being investigated clinically. A recent study on advanced HCCs described the efficacy of the combination therapy of bevacizumab, a monoclonal antibody for VEGF-A, and erlotinib, which inhibits the phosphorylation of EGFR (31). The median survival period of patients on the combination therapy was 15.6 months and appeared favorable. The dual inhibition of VEGF and EGF signaling may be more effective in the treatment of HCCs. Several reports indicated that a larger EGFR gene copy number and the presence of EGFR mutation enhanced the therapeutic efficacy of EGFR inhibitors in lung cancer and metastatic colorectal cancer (32, 33). If such predictive markers are proved to be useful in HCCs, it will be easier to select patients with HCCs who will benefit most from vandetanib. In this study, we used xenograft HCC models and thus could not evaluate the influences of cirrhosis on treatment outcome. Such model might not precisely mirror the situation of human HCCs. Another investigation using HCC model with liver cirrhosis is required before any clinical application of vandetanib is possible.

In conclusion, we have shown in this study that vandetanib, a small-molecule tyrosine kinase inhibitor of VEGFR-2 and EGFR, significantly inhibited tumor growth and intrahepatic metastasis of hepatoma cells, had no serious adverse events, and prolonged the survival time of tumor-bearing mice.

Disclosure of Potential Conflicts of Interest

M. Sata other entity (e.g., expert testimony) in MSD. No potential conflicts of interests were disclosed by the other authors.

Authors' Contributions

Conception and design: K. Inoue, T. Torimura, T. Nakamura, H. Masuda, O. Hashimoto, T. Ueno, M. Sata

Development of methodology: K. Inoue, T. Torimura, T. Nakamura, H. Masuda, M. Abe, O. Hashimoto, H. Koga, T. Ueno

Acquisition of data (provided animals, acquired and managed patients, provided facilities, etc.): K. Inoue, T. Torimura, T. Nakamura, H. Masuda, O. Hashimoto, H. Koga, T. Ueno, M. Sata

Analysis and interpretation of data (e.g., statistical analysis, biostatistics, computational analysis): K. Inoue, T. Torimura, T. Nakamura, H. Masuda, O. Hashimoto, H. Koga, T. Ueno, M. Sata

Writing, review, and/or revision of the manuscript: K. Inoue, T. Torimura, T. Nakamura, H. Masuda, O. Hashimoto, H. Koga, T. Ueno, M. Sata

Administrative, technical, or material support (i.e., reporting or organizing data, constructing databases): K. Inoue, T. Torimura, T. Nakamura, H. Iwamoto, H. Masuda, O. Hashimoto, T. Ueno, H. Yano

Study supervision: K. Inoue, T. Torimura, T. Nakamura, O. Hashimoto, T. Ueno, M. Sata

Helped in K. Inoue's experiments: H. Iwamoto

The costs of publication of this article were defrayed in part by the payment of page charges. This article must therefore be hereby marked *advertisement* in accordance with 18 U.S.C. Section 1734 solely to indicate this fact.

Received September 20, 2011; revised April 15, 2012; accepted May 11, 2012; published OnlineFirst May 18, 2012.

References

1. Yang JD, Roberts LR. Hepatocellular carcinoma: a global view. Nat Rev Gastroenterol Hepatol 2010;7:448–58.
2. Llovet JM, Ricci S, Mazzaferro V, Hilgard P, Gane E, Blanc JF, et al. Sorafenib in advanced hepatocellular carcinoma. N Engl J Med 2008;359:378–90.
3. Llovet JM, Bruix J. Testing molecular therapies in hepatocellular carcinoma: the need for randomized phase II trials. J Clin Oncol 2009;27:833–5.
4. Wilhelm SM, Carter C, Tang L, Wilkie D, McNabola A, Trail PA, et al. BAY 43–9006 exhibits broad spectrum oral antitumor activity and targets the RAF/MEK/ERK pathway and receptor tyrosine kinases involved in tumor progression and angiogenesis. Cancer Res 2004; 64:7099–109.
5. Strumberg D, Richly H, Hilger RA, Schleucher N, Korfee S, Tewes M, et al. Phase I clinical and pharmacokinetic study of the Novel Raf kinase and vascular endothelial growth factor receptor inhibitor BAY 43–9006 in patients with advanced refractory solid tumors. J Clin Oncol 2005;23:965–72.
6. Carlomagno F, Anaganti S, Guida T, Salvatore G, Troncone G, Wilhelm SM, et al. BAY 43-9006 inhibition of oncogenic RET mutants. J Natl Cancer Inst 2006;98:326–34.
7. Kirsch M, Schackert G, Black PM. Metastasis and angiogenesis. Cancer Treat Res 2004;117:285–304.
8. Geiger TR, Peeper DS. Metastasis mechanisms. Biochim Biophys Acta 2009;1793:293–308.
9. Kudo M. Early detection and characterization of hepatocellular carcinoma: value of imaging multistep human hepatocarcinogenesis. Intervirology 2006;49:64–9.
10. Miura H, Miyazaki T, Kuroda M, Oka T, Machinami R, Kodama T, et al. Increased expression of vascular endothelial growth factor in human hepatocellular carcinoma. J Hepatol 1997;27:854–61.
11. Yamaguchi R, Yano H, Iemura A, Ogasawara S, Haramaki M, Kojiro M. Expression of vascular endothelial growth factor in human hepatocellular carcinoma. Hepatology 1998;28:68–77.
12. Torimura T, Sata M, Ueno T, Kin M, Tsuji R, Sujaku K, et al. Increased expression of vascular endothelial growth factor is associated with tumor progression in hepatocellular carcinoma. Hum Pathol 1998;29: 986–91.
13. Borlak J, Meier T, Halter R, Spanel R, Spanel-Borowski K. Epidermal growth factor-induced hepatocellular carcinoma: gene expression profiles in precursor lesions, early stage and solitary tumours. Oncogene 2005;24:1809–19.
14. Thorgeirsson SS, Grisham JW. Molecular pathogenesis of human hepatocellular carcinoma. Nat Genet 2002;31:339–46.
15. Sagmeister S, Drucker C, Losert A, Grusch M, Daryabeigi A, Parzefall W, et al. HB-EGF is a paracrine growth stimulator for early tumor prestages in inflammation-associated hepatocarcinogenesis. J Hepatol 2008;49:955–64.
16. Gule MK, Chen Y, Sano D, Frederick MJ, Zhou G, Zhao M, et al. Targeted therapy of VEGFR2 and EGFR significantly inhibits growth of anaplastic thyroid cancer in an orthotopic murine model. Clin Cancer Res 2011;62:4645–55.
17. McCarty MF, Wey J, Stoeltzing O, Liu W, Fan F, Bucana C, et al. ZD6474, a vascular endothelial growth factor receptor tyrosine kinase inhibitor with additional activity against epidermal growth factor receptor tyrosine kinase, inhibits orthotopic growth and angiogenesis of gastric cancer. Mol Cancer Ther 2004;3:1041–8.
18. Yano H, Maruiwa M, Murakami T, Fukuda K, Ito Y, Sugihara S, et al. A new human pleomorphic hepatocellular carcinoma cell line, KYN-2. Acta Pathol Jpn 1988;38:953–66.
19. Yano H, Iemura A, Fukuda K, Mizoguchi A, Haramaki M, Kojiro M. Establishment of two distinct human hepatocellular carcinoma cell lines from a single nodule showing clonal dedifferentiation of cancer cells. Hepatology 1993;18:320–7.
20. Takahashi T, Yamaguchi S, Chida K, Shibuya M. A single autophosphorylation site on KDR/Flk-1 is essential for VEGF-A-dependent activation of PLC-gamma and DNA synthesis in vascular endothelial cells. EMBO J 2001;20:2768–78.

Published OnlineFirst May 18, 2012; DOI:10.1158/1078-0432.CCR-11-2041

21. O'Reilly MS, Holmgren L, Shing Y, Chen C, Rosenthal RA, Moses M, et al. Angiostatin: a novel angiogenesis inhibitor that mediates the suppression of metastases by a Lewis lung carcinoma. Cell 1994;79: 315–28.
22. Sasaki S, Ishida T, Toyota M, Ota A, Suzuki H, Ashida M, et al. Interferon-α/β and anti-fibroblast growth factor receptor 1 monoclonal antibody suppress hepatic cancer cells *in vitro* and *in vivo*. PLoS One 2011;6:e19618.
23. Stock P, Monga D, Tan X, Micsenyi A, Loizos N, Monga SP. Platelet-derived growth factor receptor alpha: a novel therapeutic target in human hepatocellular cancer. Mol Cancer Ther 2007;6:1932–41.
24. Wedge SR, Ogilvie DJ, Dukes M, Kendrew J, Chester R, Hennequin LF. ZD6474 inhibits vascular endothelial growth factor signaling, angiogenesis, and tumor growth following oral administration. Cancer Res 2002;62:4645–55.
25. Giannelli G, Azzariti A, Sgarra C, Porcelli L, Antonaci S, Paradiso A. ZD6474 inhibits proliferation and invasion of human hepatocellular carcinoma cells. Biochem Pharmacol 2006;71:479–85.
26. Arao T, Fukumoto H, Takeda M, Tamura T, Saijo N, Nishio K. Small in-frame deletion in the epidermal growth factor receptor as a target for ZD6474. Cancer Res 2004;64:9101–4.
27. Saaristo A, Karpanen T, Alitalo K. Mechanisms of angiogenesis and their use in the inhibition of tumor growth and metastasis. Oncogene 2000;19:6122–9.
28. Matsuo, Sakurai H, Saiki I. ZD1839, a selective epidermal growth factor receptor tyrosine kinase inhibitor, shows antimetastatic activity using a hepatocellular carcinoma model. Mol Cancer Ther 2003;2:557–61.
29. Holmgren L, O'Reilly MS, Folkman J. Dormancy of micrometastases: balanced proliferation and apoptosis in the presence of angiogenesis suppression. Nat Med 1995;1:149–53.
30. Natale RB, Badkin D, Govinndan R, Sleckman GB, Rizvi NA, Capo A, et al. Vandetanib versus gefitinib in patients with advanced non-small-cell lung cancer: results from a two-part, double-blind, randomized phase II study. J Clin Oncol 2009;27:2523–9.
31. Thomas MB, Morris JS, Chadha R, Iwasaki M, Kaur H, Lin E, et al. phase II trial of the combination of bevacizumab and erlotinib in patients who have advanced hepatocellular carcinoma. J Clin Oncol 2009;27:843–50.
32. Linardou H, Dahabreh IJ, Kanaloupiti D, Siannis F, Bafaloukos D, Kosmidis P, et al. Assessment of somatic k-RAS mutations as a mechanism associated with resistance to EGFR-targeted agents: a systematic review and meta-analysis of studies in advanced non-small-cell lung cancer and metastatic colorectal cancer. Lancet Oncol 2008;9:962–72.
33. Gazdar AF. Personalized medicine and inhibition of EGFR signaling in lung cancer. N Engl J Med 2009;361:1018–20.

Hepatology Research

Hepatology Research 2012; 42: 591–600 doi: 10.1111/j.1872-034X.2011.00953.x

Original Article

Hepatitis C virus core protein upregulates the expression of vascular endothelial growth factor via the nuclear factor-κB/hypoxia-inducible factor-1α axis under hypoxic conditions

Mitsuhiko Abe,[1] Hironori Koga,[1] Takafumi Yoshida,[1] Hiroshi Masuda,[1] Hideki Iwamoto,[1] Masahiro Sakata,[1] Shinichiro Hanada,[1] Toru Nakamura,[1] Eitaro Taniguchi,[1] Takumi Kawaguchi,[1] Hirohisa Yano,[2] Takuji Torimura,[3] Takato Ueno[4] and Michio Sata[1,3]

[1]*Division of Gastroenterology, Department of Medicine,* [2]*Department of Pathology, Kurume University School of Medicine,* [3]*Research Center for Innovative Cancer Therapy, Kurume University, Kurume and* [4]*Asakura Medical Association Hospital, Asakura, Japan*

Aim: Hepatitis C virus (HCV) core protein critically contributes to hepatocarcinogenesis, which is often observed in liver cirrhosis. Since the liver cirrhosis microenvironment is affected by hypoxia, we focused on the possible driving force of HCV core protein on signal relay from hypoxia-inducible factor (HIF)-1α to vascular endothelial growth factor (VEGF).

Methods: Human hepatocellular carcinoma cells stably overexpressing HCV core (Core cells) and NS5A (NS5A cells) were established; empty vector-transfected (EV) cells were used as controls. Hypoxia was induced by oxygen deprivation or by using cobalt chloride ($CoCl_2$). YC-1 was used to inhibit HIF-1α expression. Protein analyses for cultured cells and liver tissues obtained from $CoCl_2$-treated HCV core-transgenic (Core-Tg) mice were performed by western blot and/or immunocytochemistry. Cellular mRNA levels were evaluated by quantitative real-time reverse transcription-polymerase chain reaction.

Results: Under hypoxia, the sustained expression of HIF-1α, but not HIF-2α, was profoundly observed in Core cells but, was faint in EV and NS5A cells. Immunocytochemistry revealed increased HIF-1α in the nucleus. HIF-1α mRNA levels were significantly higher in Core cells than in EV cells under both normoxia and hypoxia. The HIF-1α-targeted VEGF and Bcl-xL expressions were increased in Core cells under hypoxia and abolished by YC-1 treatment. Hypoxic liver samples of Core-Tg mice indicated significant increases in both HIF-1α and VEGF expression compared with the wild type.

Conclusions: Hepatitis C virus core protein has the distinct potential to transcriptionally upregulate and sustain HIF-1α expression under hypoxia, thereby contributing to increased VEGF expression, a key regulator in the hypoxic milieu of liver cirrhosis.

Key words: hepatocellular carcinoma, hypoxia, transgenic mouse

INTRODUCTION

HEPATITIS C VIRUS (HCV) is one of the major pathogens that cause chronic liver diseases, including liver cirrhosis; liver cirrhosis facilitates the development of hepatocellular carcinoma (HCC) with an annual incidence of 7.9% in stage F4 liver cirrhosis.[1] Despite intensive research, the underlying mechanism of HCV-related HCC development remains unclear. Among HCV proteins, including structural (i.e., core, E1, E2, and p7) and nonstructural (i.e., NS2, NS3, NS4A, NS4B, NS5A, and NS5B) proteins, HCV core protein is suggested to play an important role in hepatocarcinogenesis.[2] Although the oncogenic effect of the protein on cellular DNA is unclear, its direct interaction with some transcription factors such as signal transducer and activator of transcription (STAT)3 and sterol

Correspondence: Dr Hironori Koga, Division of Gastroenterology, Department of Medicine, Kurume University School of Medicine, 67 Asahi-machi, Kurume 830-0011, Japan. Email: hirokoga@med.kurume-u.ac.jp

Received 1 October 2011; revision 17 November 2011; accepted 28 November 2011.

regulatory element-binding protein (SREBP)-1c are suggested to strongly promote and modulate the carcinogenesis process.[3,4]

In cirrhotic livers, blood supply is impaired as a consequence of fibrosis, which induces a hypoxic microenvironment in the liver.[5] Indeed, a previous study demonstrates that the expression level of hypoxia-inducible factor-1α (HIF-1α), a nuclear transcription factor, gradually increases with the degree of fibrosis.[6] Under normoxic conditions, HIF-1α is proline hydroxylated by HIF hydroxylase, resulting in degradation via the ubiquitin-proteasomal pathway, which involves von Hippel-Lindau (VHL) protein. In contrast, HIF-1α is stabilized under hypoxia due to less hydroxylation; it reaches the nucleus, where it transactivates a variety of genes related to angiogenesis, glucose metabolism, cell proliferation, and anti-apoptosis.[7]

In this context, the mechanistic link between HCV infection and HIF-1α-mediated cellular responses was recently examined.[8,9] It is reported that HCV upregulates the expression level of HIF-1α protein, thereby leading to an increase in VEGF production and alterations to glucose metabolism.[8,9] However, it is not known which component protein of HCV is the main cause of HIF-1α upregulation. Thus, the aim of the present study was to assess the possible involvement of HCV core protein in the hypoxic cellular responses, including angiogenesis, in comparison to NS5A protein, which is another potentially oncogenic viral component.[10,11]

METHODS

Materials

THE HIF-1A INHIBITOR, YC-1, was purchased from Sigma (St. Louis, MO, USA). The nuclear factor-κB (NF-κB) activation inhibitor, JSH-23, and the STAT3 inhibitor, S3I-201, were from Calbiochem (San Diego, CA, USA). The SP1 inhibitor, mithramycin, was obtained from Santa Cruz Biotechnology (Santa Cruz, CA, USA). Cycloheximide was from Wako Pure Chemical Industries (Osaka, Japan). The primary antibodies used were directed against vascular endothelial growth factor (VEGF), Flk-1 (VEGFR2), and Lamin A/C (Santa Cruz Biotechnology); HIF-1α (clone 54) (BD Biosciences, Franklin Lakes, NJ, USA); HIF-2α, and HCV core (Abcam, Cambridge, MA, USA); p-VEGFR2 (Tyr1175), Bcl-xL, and c-Myc (Cell Signaling Technology, Beverly, MA, USA); FLAG (M2) and actin (Sigma); and c-myc tag antibody (Nacalai Tesque, Kyoto, Japan). Enhanced chemiluminescence reagents were obtained from Amersham Pharmacia (Buckinghamshire, UK), and the protein assay reagents were from Bio-Rad (Hercules, CA, USA). All other reagents and compounds were of analytical grade.

Cell lines and culture

Human hepatoma cell line HAK-1A and human umbilical vein endothelial cells (HUVECs) were used in this study. HAK-1A resembles well-differentiated HCC cells and was established from an HCV-related cirrhotic patient.[12] This cell line was grown in Dulbecco's modified Eagle medium (Wako Pure Chemical Industries) supplemented with 10% heat-inactivated (56°C for 30 min) fetal bovine serum (FBS) (BioWest, Nuaille, France), 100 units/mL penicillin, and 100 μg/mL streptomycin (Nacalai Tesque) in a humidified atmosphere of 5% CO_2 at 37°C. HUVECs were purchased from Lonza (Walkersville, MD, USA) and cultured in EGM-2-based medium. Cell culturing under hypoxic conditions (1% oxygen) was performed using an APM-30D incubator with an oxygen concentration regulator system (ASTEC, Fukuoka, Japan). Alternatively, cells were exposed to the hypoxia-mimicking chemical cobalt chloride ($CoCl_2$; Nacalai Tesque).[13]

Transfection of cDNA and establishment of stable cell lines

The pcDNA3.1-based plasmid harboring HCV core cDNA (myc-tagged) was created as described previously.[3] The FLAG-tagged NS5A of the HCV (genotype 1b) expression plasmid was kindly provided by Dr Naoya Sakamoto (Tokyo Medical and Dental University, Japan). To generate stable transfectants, HAK-1A cells were transfected with HCV core, NS5A, or empty vector (EV) plasmid using the TransIT-LT1 Reagent (Mirus Bio Corporation, Madison, WI, USA), according to the manufacturer's instructions. HCV core-myc- and NS5A-FLAG-overexpressing clones as well as mock-transfected cells were selected by G418 (800 μg/mL) and maintained in 400 μg/mL of G418 (Nacalai Tesque).

Western blot analysis

Cells were lysed in RIPA buffer (Pierce, Rockford, IL, USA) containing 1 mmol/L ethylenediaminetetraacetic acid (EDTA) (pH 8.0), 0.1 mmol/L sodium fluoride (NaF), 0.1 mmol/L sodium orthovanadate (Na_3VO_4), 100 mmol/L phenylmethylsulfonyl fluoride (PMSF), 1 mmol/L dithiothreitol (DTT), 2 × Protease Inhibitor

Cocktail (Nacalai Tesque), and 2 × Halt Phosphatase Inhibitor Cocktail (Pierce). The lysates were centrifuged at 19 300 *g* for 20 min at 4 °C, and the supernatants were separated. For nuclear/cytoplasmic fractionation, NE-PER extraction reagent (Pierce) was used according to the manufacturer's protocol. Liver tissues obtained from mice were homogenized by a TissueLyser (Qiagen, Valencia, CA, USA) in cold lysis buffer, and the homogenates were clarified by centrifugation. Protein concentrations were measured using a Bio-Rad protein assay kit. After being boiled for 5 min in the presence of 2-mercaptoethanol, samples containing cell or tissue lysate proteins were separated on 8% or 10% sodium dodecyl sulfate (SDS)-polyacrylamide gels and subsequently transferred onto equilibrated polyvinylidene difluoride (PVDF) membranes (Bio-Rad). Proteins of the whole-cell lysates (35 μg) as well as 25 μg nuclear and 35 μg cytoplasmic protein samples were applied to each lane on the gels. After masking by Protein-Free T20 (TBS) Blocking Buffer (Pierce), the membranes were incubated with the primary antibodies described above. The bound antibodies were detected with horseradish peroxidase (HRP)-labeled sheep anti-mouse IgG or HRP-labeled donkey anti-rabbit IgG (Amersham Pharmacia Biotech) using the enhanced chemiluminescence detection system (ECL Advanced kit). Positive signals from the target proteins were visualized using an image analyzer (LAS-4000; Fujifilm, Tokyo, Japan). Densitometry for the signals was performed using Multi Gauge version 3.0 software (Fujifilm).

Immunofluorescence confocal laser scanning microscopy

Cells grown on 35-mm diameter glass-bottom dishes (MatTek, Ashland, MA, USA) were fixed with cold acetone/methanol (1:1) for 5 min, and subsequently washed in PBS containing 0.05% Tween 20 (PBS-T). Nonspecific reactions were blocked with Protein Block Serum-Free (DAKO North America, Carpinteria, CA, USA) and then incubated with anti-HIF-1α antibody overnight at 4 °C. After washing in PBS-T, the specimens were treated with Alexa Fluor goat anti-mouse IgG (H + L) antibody (Molecular Probes, Eugene, OR, USA) for 40 min at room temperature. Then, after their RNA was digested by RNase (Nippon Gene, Tokyo, Japan), the specimens were counterstained with propidium iodide (PI). A confocal laser scanning microscope (FLUOVIEW FV300; Olympus, Tokyo, Japan) equipped with an argon/krypton laser capable of dual excitation and detection was used to observe the immunostaining for the protein and the nuclear localization of PI.

Quantitative real-time RT-PCR

To analyze HIF-1α and HIF-2α mRNA expressions, total RNA was isolated from cells using TRIzol reagent (Invitrogen, Carlsbad, CA, USA). RNA was quantified by spectrophotometry. Real-time polymerase chain reaction (PCR) amplification was conducted using an ABI 7500 Real-Time PCR System instrument and software (Applied Biosystems, Tokyo, Japan). The following primer sets were used: GAPDH control forward: 5′-CATGAGAAGTATGACAACAGCC-3′, GAPDH control reverse: 5′-AGTCCTTCCACGATACCAAAG-3′; HIF-1α forward: 5′-TGCTCATCAGTTGCCACTTCC-3′, HIF-1α reverse: 5′-CCAAATCACCAGCATCCAGAAGT-3′; HIF-2α forward: 5′-AGTGCATCATGTGTGTCAACTACG-3′, HIF-2α reverse: 5′-GGGCTTGAACAGGGATTCAGTC-3′. The PCR conditions and cycles were as follows: initial denaturation for 10 min at 95 °C, followed by 40 cycles of denaturation at 95 °C for 15 s and annealing/extension at 60 °C for 60 s. Experiments were performed at least three times. The data are expressed as the fold changes of HCV core-overexpressing cells (Core cells) relative to mock-transfected cells (EV cells) using the Delta-Delta method. Relative gene expressions were normalized to that of GAPDH.

Cell-cycle analysis by flow cytometry

DNA content was assessed by staining ethanol-fixed cells with PI and monitoring using a FACS Calibur (Becton Dickinson, Franklin Lakes, NJ, USA). The percentages of cells in the S, G_0/G_1, and G_2/M phases of the cell cycle were determined using ModFit software (Verity Software House, Topsham, ME, USA).

Cell proliferation assay

Cells (1×10^4) were seeded onto three wells in 6-well plates with or without 160 μM $CoCl_2$. After the cells were cultured for 8 days, the numbers of cells in 12 wells were counted in duplicate using a CDA-500 automated cell counter (Sysmex, Kobe, Japan).

VEGFR2 phosphorylation assay

To examine if VEGF produced by the cells under hypoxic conditions was secreted into the culture media and biologically active, serum-free culture supernatants were collected from the $CoCl_2$-treated cells and allowed to stimulate VEGFR2 in HUVECs for 10 min.

HCV core-transgenic (Tg) mice and $CoCl_2$ treatment

The HCV core-Tg mice were kindly provided by Dr Takeshi Tokuhisa (Chiba University, Japan). To determine the possible driving force of HCV core protein on the HIF-1α/VEGF axis *in vivo*, 16-week-old male Core-Tg mice (Core-Tg) and wild-type control mice (Wild) were given a single intraperitoneal injection of $CoCl_2$ at 60 μg/g body weight and killed 6 h later as described previously.[14,15] Liver tissues were subjected to western blot analysis. All animal experiments were conducted in accordance with the NIH Guidelines for the Care and Use of Laboratory Animals and were approved by the University of Kurume Institutional Animal Care and Use Committee.

Statistical analysis

Statistical significance was assessed using the Mann–Whitney *U*-test. $P < 0.05$ was considered statistically significant.

RESULTS

HCV core enhances the hypoxia-induced expression of HIF-1α protein

WE ESTABLISHED HAK-1A-BASED cell clones stably overexpressing HCV core protein (Core cells) and NS5A protein (NS cells) (Fig. 1a). Stable transfectants with empty vector plasmid cDNA (EV cells) were used as controls. When Core and EV cells were exposed to 1% O_2 for 6 h, Core cells expressed more HIF-1α than EV cells did, although only a slight increase in HIF-2α expression was observed in Core cells (Fig. 1b). Since HIF-α proteins, including HIF-1α, are transcription factors and are known to function in the nucleus, we confirmed the nuclear localization of HIF-1α under hypoxic conditions by immunocytochemistry using 160 μM $CoCl_2$ (Fig. 1c). Furthermore, western blot analysis in combination with nuclear/cytoplasmic fractionation was used to strengthen the predominant nuclear upregulation of HIF-1α in Core cells under hypoxic conditions (Fig. 1d). It was evident that nuclear upregulation in hypoxic Core cells was unique to HIF-1α and not HIF-2α. Next, we tested if other HCV-derived proteins including NS5A, which is also suggested to have oncogenic potential like HCV core protein,[10,11] exhibited similar effects. However, NS5A overexpression under hypoxic conditions caused no clear increase in HIF-1α (Fig. 1e).

HIF-1α degradation was not retarded in Core cells

The intracellular amount of HIF-1α is balanced between its production and degradation; degradation is tightly regulated by the ubiquitin-proteasomal pathway. Thus, to examine initially whether HCV core upregulates the expression level of HIF-1α by directly inhibiting the degradation pathway, we chased the protein expression levels after inhibiting protein synthesis using cycloheximide (CHX) under hypoxic conditions. HIF-1α expression levels decreased 30 and 60 min after treating cells with 5 μg/mL CHX to 36% and 65% in EV cells and 42% and 60% in Core cells, respectively. These results suggest that the degradation efficiency of the protein is not lowered by HCV core protein (Fig. 2).

HCV core transcriptionally upregulated HIF-1α expression

To investigate whether HIF-1α is transcriptionally upregulated in Core cells, we performed quantitative real-time reverse transcription (RT)-PCR to measure HIF-1α mRNA levels. The transcriptional levels of HIF-1α in Core cells were significantly higher than those in EV cells under both normoxic and hypoxic conditions. Consistent with the protein analysis results in this study, the transcriptional levels of HIF-2α were not significantly different between Core and EV cells (Fig. 3a). Since recent data suggest that distinct transcription factors such as NF-κB, SP-1, and STAT3 directly control HIF-1α mRNA synthesis,[16–19] we explored which factor(s) contributed most to the upregulation of HIF-1α by using specific inhibitors against these three transcription factors. Under hypoxic conditions, the upregulated HIF-1α protein expression in Core cells was suppressed by the NF-κB activation inhibitor, JSH-23 (30 μM), but not by the SP-1 inhibitor, mithramycin (100 nM), or the STAT3 inhibitor, S3I-201 (100 μM) (Fig. 3b). When the concentration of JSH-23 was increased to 60 μM under hypoxic conditions, the upregulated HIF-1α protein expression was clearly abolished in concert with the decreased expression of NF-κB (Fig. 3c). These findings strongly suggest that HCV core elevates the mRNA expression levels of HIF-1α by activating the NF-κB signaling pathway.

HCV core-induced HIF-1α increased VEGF expression under hypoxia

Since HIF-1α regulates a diverse range of cellular events, including cell proliferation, angiogenesis, and

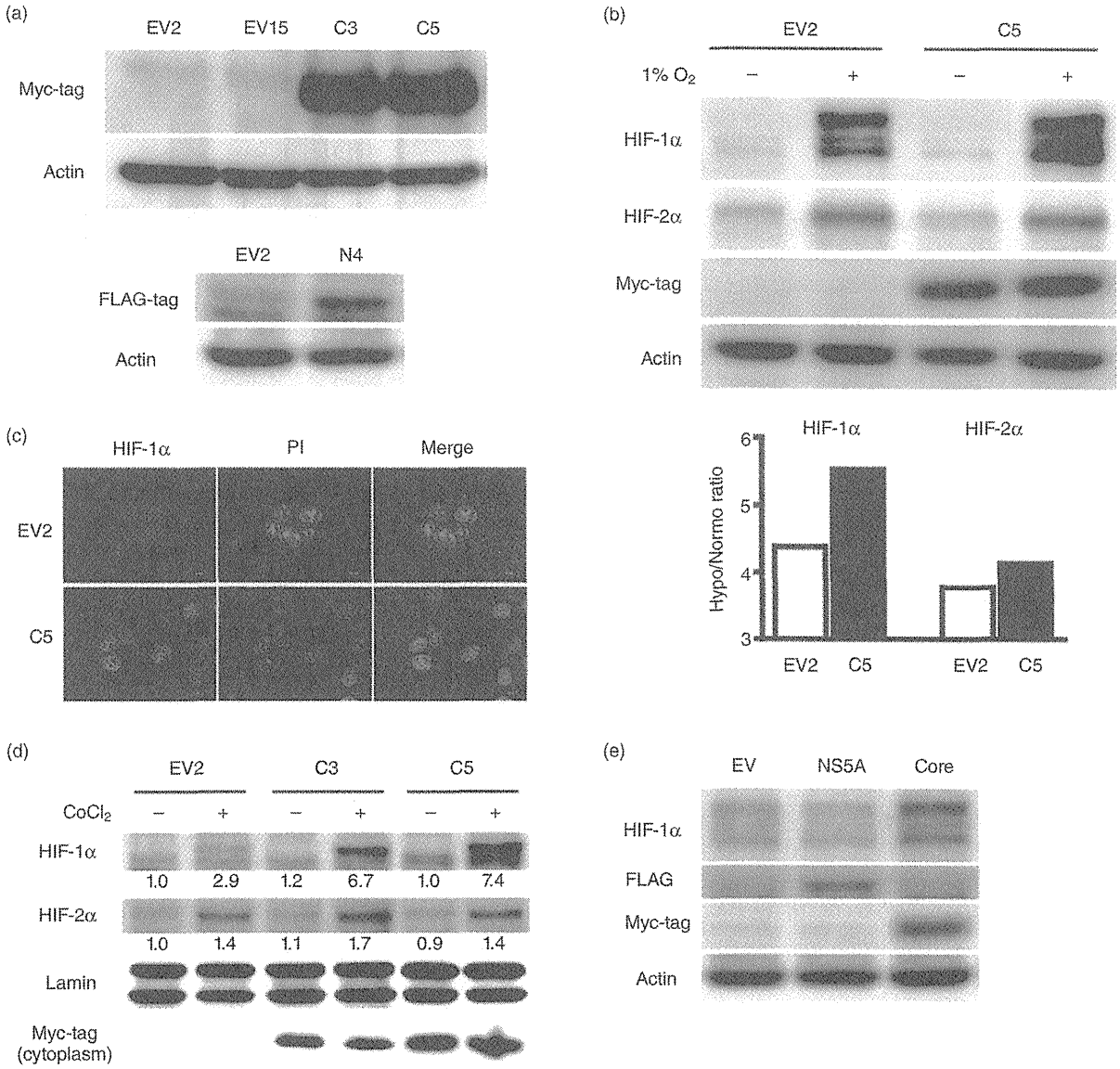

Figure 1 Preferential induction of hypoxia-inducible factor (HIF)-1α via hepatitis C virus (HCV) core under hypoxia. (a) Western blot analysis of stable cell lines. Positive signals for Myc-tag (HCV core) and FLAG-tag (HCV NS5A) are shown in clones C3 and C5, and N4, respectively. EV2 and EV15, empty vector (EV)-transfected HAK-1A cell clones 2 and 15. (b) EV2 and C5 were exposed to 20% and 1% O_2 for 6 h, respectively. The protein expression levels of HIF-1α and HIF-2α were examined by western blot analysis. Protein (35 μg) of whole-cell lysates was applied to each lane. Lower graph shows densitometric ratios of HIF protein expressions under hypoxia (Hypo) to those under normoxia (Normo). (c) Confocal laser scanning microscopy for the nuclear localization of HIF-1α protein under hypoxic conditions. (d) EV2, C3, and C5 cells were treated with or without 160 μM $CoCl_2$ for 24 h, and their nuclear extracts were subjected to western blot analysis for HIF-1α and HIF-2α. Lamin A/C (Lamin) was used as a control protein to monitor valid nuclear/cytoplasmic fractionation. Relative densitometric values for HIF-1α and HIF-2α expression levels are presented beneath the corresponding bands. (e) Comparison of HIF-1α protein expression levels among EV (EV2), NS5A (N4), and Core (C5) cells by western blot analysis. Whole-cell lysates from the cells exposed to 160 μM $CoCl_2$ for 24 h were used.

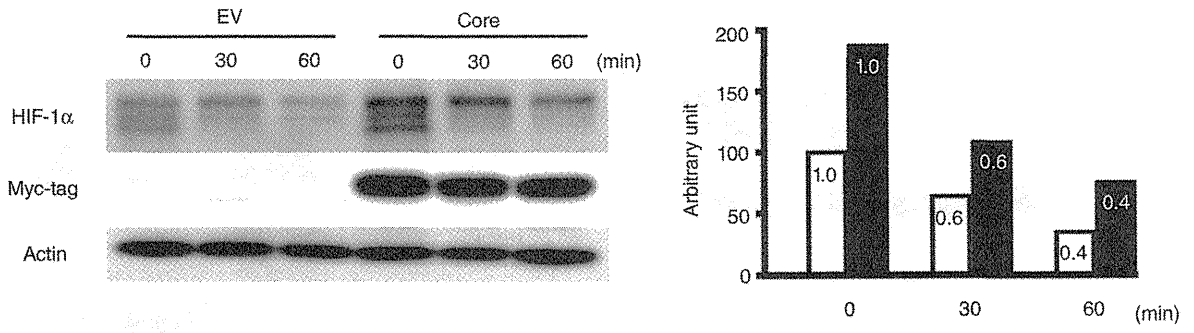

Figure 2 Hepatitis C virus (HCV) core does not promote hypoxia-inducible factor (HIF)-1α degradation. EV (EV2) and Core (C5) were exposed to 5 μg/mL cycloheximide (CHX) for 0, 30, or 60 min at the last phase of the 24-h $CoCl_2$ treatment. Whole-cell lysates were used for western blot analysis to evaluate HIF-1α expression levels after protein synthesis was inhibited by CHX administration. Right panel shows densitometric values (time 0 = 1.0) for the HIF-1α expression levels. □, Ev; ■, Core.

anti-apoptosis, the net effects resulting from increased intracellular HIF-1α were compared between Core and EV cells. In cell cycle analyses, Core cells exhibited a slight decrease in the number of cells in the S phase compared with EV cells under hypoxia; however, Core cells also demonstrated a similar increase under normoxia (Fig. 4a). This finding led to a similar but significant difference in the actual cell number at culture day 8 (Fig. 4b). Taken together, these results suggest that HCV core-induced HIF-1α expression under hypoxia confers anti-proliferative activity to liver cancer cells. Next, we evaluated if VEGF and Bcl-xL are upregulated in Core cells under hypoxic conditions, since they are downstream gene products of HIF-1α. As expected, the expression levels of both proteins were elevated in Core cells under hypoxia, followed by the upregulation of HIF-1α (Fig. 4c). It is worth noting that when the cells were incubated with the HIF-1α inhibitor, YC-1 (10 μM), the elevations in VEGF and Bcl-xL expression were clearly abolished according to the diminished HIF-1α expression; this suggests that the induced HIF-1α plays roles in angiogenesis and anti-apoptosis in Core cells under hypoxia (Fig. 4c). To assess whether VEGF produced by the Core cells was secreted into the culture media and if it was biologically functional, whether the supernatants of the cells caused VEGFR2 phosphorylation in HUVECs was tested. Only the supernatants from Core cells induced clear VEGFR2 phosphorylation at Tyr^{1175}, which is a hallmark of the activation of the VEGFR signaling pathway (Fig. 4d). On the other hand, supernatants from EV and NS5A cells failed to increase the Tyr^{1175}-phosphorylated VEGFR2 protein expression in HUVECs (Fig. 4d).

Predominant induction of HIF-1α expression in HCV core-transgenic mice

To determine whether HCV core-related HIF-1α upregulation really occurs in hypoxic livers, protein extracts were obtained from the livers of Core-Tg and Wild mice that received equal treatment with intraperitoneal $CoCl_2$. Although there were slight variations in the expression levels in HIF-1α and VEGF among the

Figure 3 Involvement of nuclear factor-κB (NF-κB) in the hepatitis C virus (HCV) core-mediated hypoxia-inducible factor (HIF)-1α upregulation. (a) Quantitative real-time reverse transcription-polymerase chain reaction (RT-PCR) analysis for HIF-1α and HIF-2α mRNA expression levels. Total RNA was extracted from EV (EV2) and Core (C5) cells 24 h after 160 μM $CoCl_2$ treatment. The RT-PCR products of glyceraldehyde 3-phosphate dehydrogenase (GAPDH) were chosen as an internal standard for RNA quantity and integrity. Ratios of HIF-1α and HIF-2α mRNA levels to those of GAPDH are expressed as mean (SD) ($n = 6$). n.s., not significant. (b) EV and Core cells were treated with JSH-23 (30 μM), mithramycin (100 nM), or S3I-201 (100 μM) for 24 h under $CoCl_2$-induced hypoxic conditions. Nuclear extracts obtained from the cells were subjected to western blot analysis for the indicated molecules. (c) NF-κB expression level was suppressed in the Core cells treated with 60 μM JSH-23. Nuclear extracts of the cells were used for western blot analysis. Densitometry results regarding HIF-1α band intensity are presented (right panel). Percentages are decreased rates in the densitometric values after JSH-23 treatment. Nuc, nuclear; Cyto, cytoplasmic; Inhib, inhibitor (JSH-23).

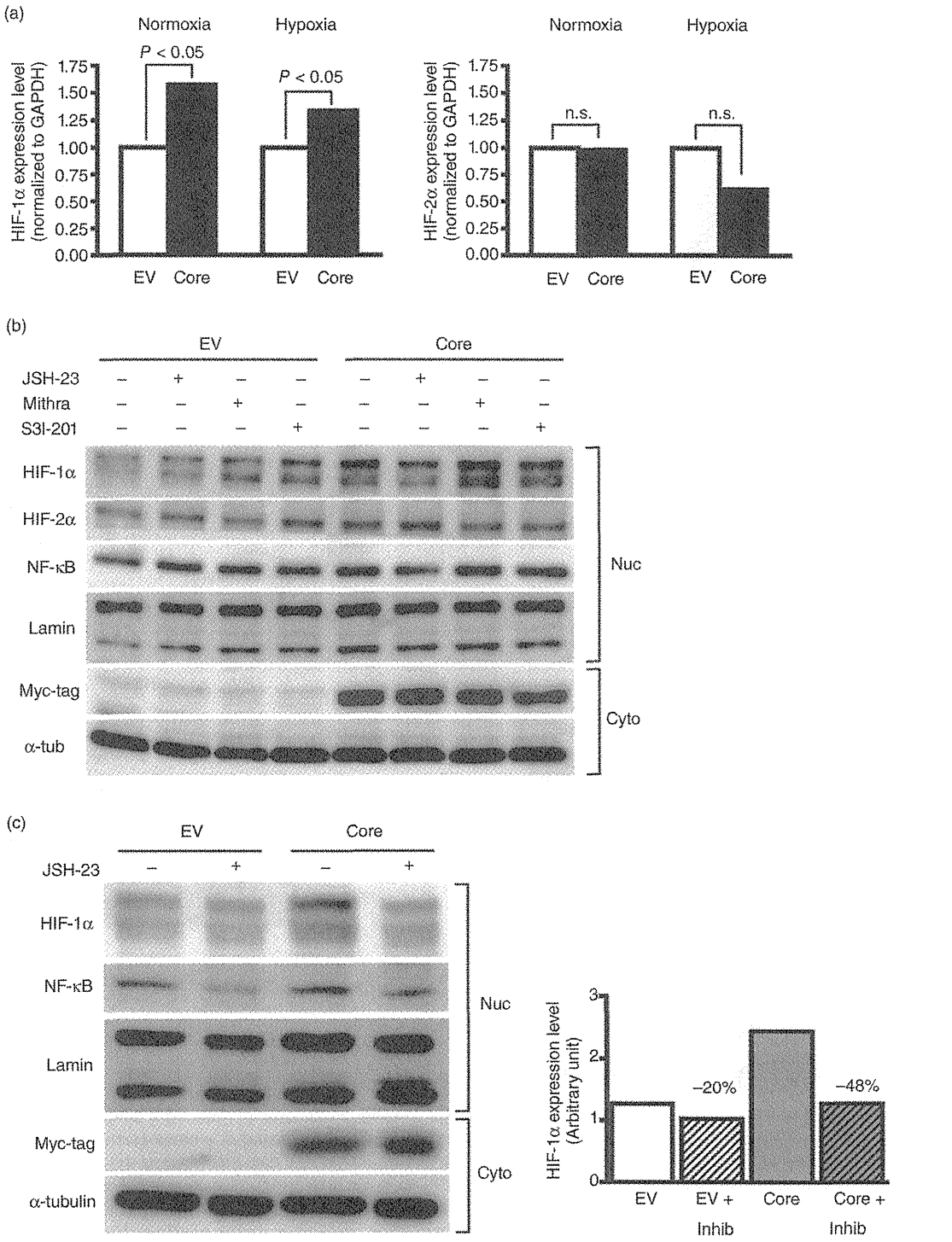

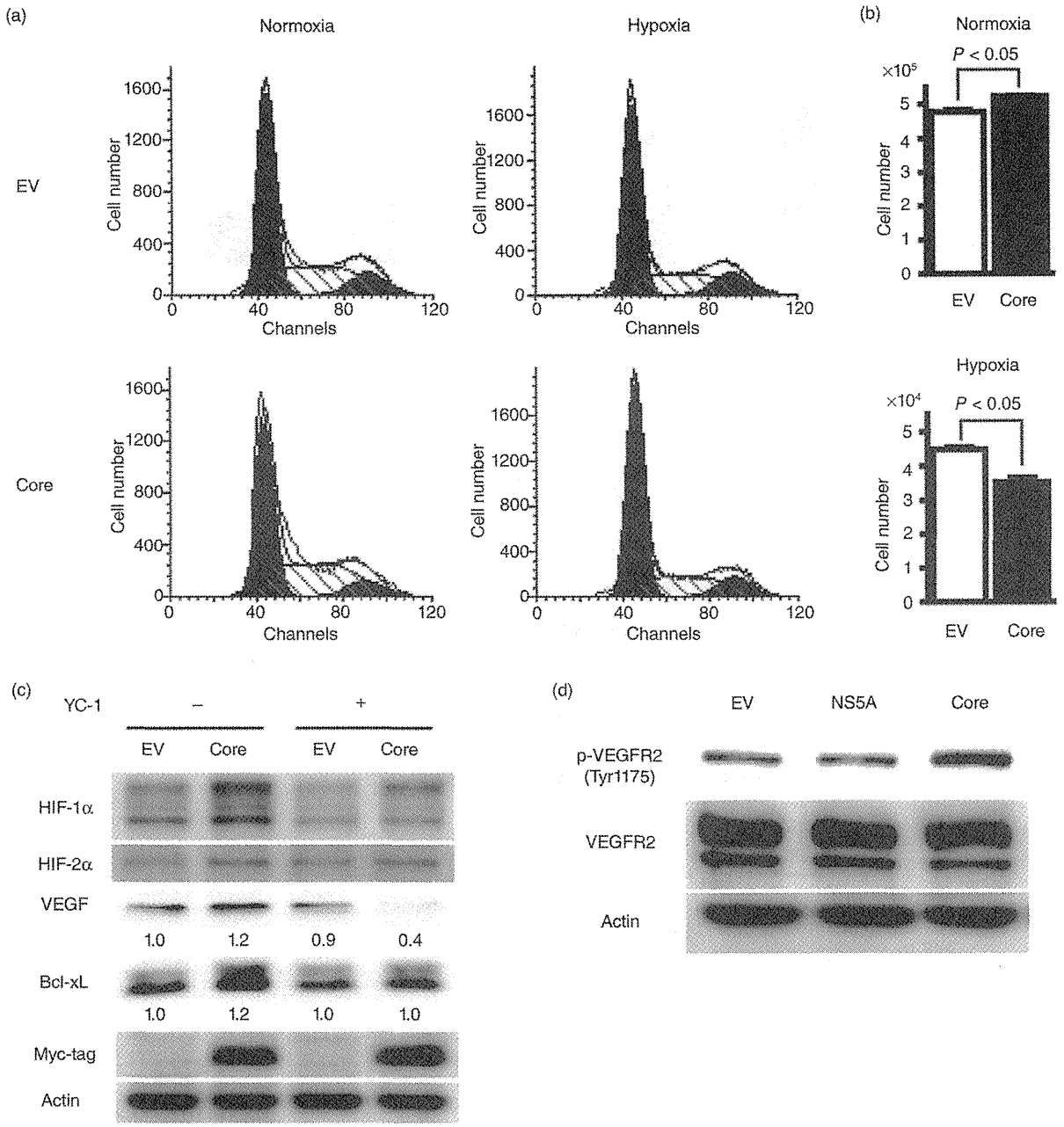

Figure 4 Increased functional vascular endothelial growth factor (VEGF) production in Core cells under hypoxia. (a) Flow cytometric analysis of the cell cycle in EV (EV2) and Core (C5) cells treated with (hypoxia) or without (normoxia) 160 μM $CoCl_2$ for 24 h. (b) Machine-counted numbers of EV and Core cells with or without $CoCl_2$ 8 days after seeding. (c) Western blot analysis focusing on the expression levels of hypoxia-inducible factor (HIF)-1α target gene products such as VEGF and Bcl-xL. Cells were treated with or without 10 μM YC-1 for 10 h under the $CoCl_2$-induced hypoxic conditions. Relative densitometric values for VEGF and Bcl-xL expression levels are presented beneath the corresponding bands. (d) Human umbilical vein endothelial cells (HUVECs) were cultured in serum-free spent media obtained from culture dishes for EV (EV2), NS5A (N4), and Core (C5) cells. The expression levels of Tyr^{1175}-phosphorylated (p-) VEGFR2 and total VEGFR2 were evaluated by western blot analysis.

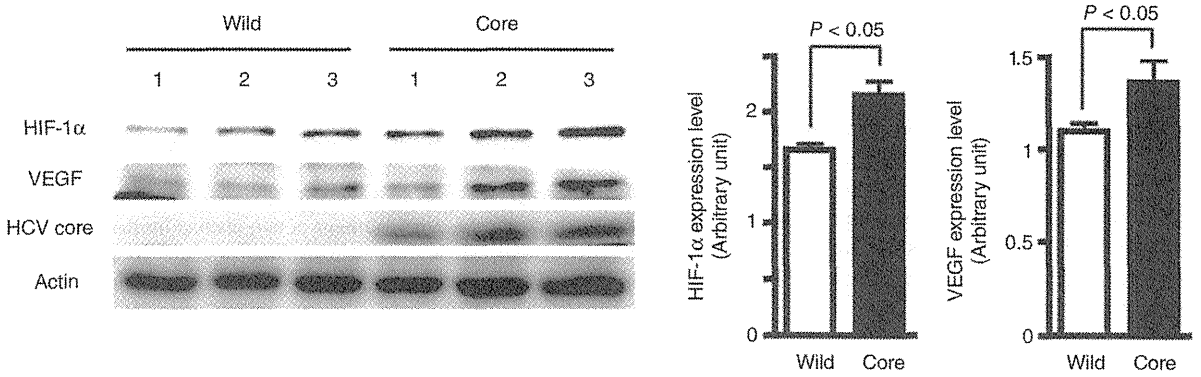

Figure 5 Comparison of the expression levels of hypoxia-inducible factor (HIF)-1α and vascular endothelial growth factor (VEGF) between wild-type (Wild) and Core-Tg (Core) mice treated with an intraperitoneal injection of $CoCl_2$ (60 μg/g body weight). The mice were killed 6 h after injection. Protein extracts from the liver tissues were subjected to western blot analysis. Densitometric analysis of visualized bands for HIF-1α and VEGF was performed.

animals in each group, both protein levels were significantly higher in Core-Tg than in Wild mice after $CoCl_2$ administration (Fig. 5). These findings suggest that the HCV core-involved hypoxic response is universal, even *in vivo*.

DISCUSSION

THE RESULTS OF the present study demonstrate the following: (i) HCV core protein preferentially induces high expression levels of HIF-1α protein in hepatocyte-derived cells under hypoxic conditions; (ii) NF-κB-mediated transcriptional upregulation but not attenuated protein degradation contributes to the HIF-1α expression augmented by HCV core protein; (iii) one of the important biological consequences of the increased HIF-1α is the production of active VEGF, which leads to VEGFR2 activation in endothelial cells; and (iv) the hypoxic livers of Core-Tg mice exhibit significantly higher HIF-1α expression levels.

Previous studies suggest that HCV plays a role in upregulating HIF-1α expression;[8,9] however, these studies do not focus on the involvement of specific HCV proteins involved in HIF-1α upregulation. On this point, the present study demonstrates that HCV core is responsible for the upregulation of HIF-1α. Furthermore, the expression mode of HIF-1α protein differs between the previous and present reports, in that the HCV-related HIF-1α increase was observed even under normoxia in the previous reports but, strictly under hypoxia in the present report. This discrepancy might be derived from differences in HCV-related materials and/or the cell lines used. In the present study, it is worth noting that NS5A, another potentially oncogenic protein of HCV,[10,11] did not induce HIF-1α upregulation under hypoxia, suggesting that HCV core protein contributes more to hepatocarcinogenesis under hypoxia via angiogenesis, a fundamental biological event in the microenvironment of cirrhotic liver.[5,6]

Our results suggest that the HCV core/NF-κB axis plays a significant role in HIF-1α augmentation. The role of this axis seems reasonable, since it is known that HCV core activates NF-κB in several other cell systems.[20,21] Other transcription factors known to upregulate HIF-1α, such as SP-1 and STAT3, were not involved in the HCV core-augmented HIF-1α expression under hypoxia in this study. Determining the detailed mechanism of the distinct collaborative role of NF-κB and HCV core in upregulating HIF-1α requires further investigation.

Among the HIF-1α-regulated diverse cellular events, including angiogenesis, proliferation, apoptosis/survival, and metabolism, angiogenesis was found to be a major biological output in Core cells under hypoxia. Indeed, the results of this study demonstrate that HCV core-induced HIF-1α activates the VEGFR2 signaling pathway in endothelial cells via VEGF secreted by the Core cells under hypoxic conditions. The distinct angiogenic potential of HCV core protein under hypoxia might help transformed cells survive in the hypoxic milieu of the cirrhotic liver by supplying them with oxygen and nutrients. HCV is known to be able to replicate in HCC tissue;[22] however, the viral load is estimated to be lower than that in surrounding noncan-